COLOR HIGH DYNAMIC RANGE (HDR) IMAGING: THE LUMINANCE-CHROMINANCE APPROACH

Ossi Pirinen, Alessandro Foi, Atanas Gotchev

Institute of Signal Processing

Tampere University of Technology, Finland

firstname.lastname@tut.fi

ABSTRACT

This paper presents a novel and efficient approach to color in high dynamic range (HDR) imaging. In contrast to state-of-the-art methods, we propose to move the complete HDR imaging process from RGB to a luminance-chrominance color space. Our aim is to get a computationally efficient technique and to avoid any possible color distortions originating from the three RGB color channels processed separately. To achieve this, we build a camera response function for the luminance channel only and weight and compose the HDR luminance accordingly, while for the chrominance channels we apply weighting in relation with the saturation level. We demonstrate that our technique yields natural and pleasant to perceive tone-mapped images and is also more robust to noise.

1. INTRODUCTION

Visual representation of natural scenes has reached a point where spatial resolution is no longer an issue and greater realism is achieved by either adding the third dimension or utilizing a more and more realistic gamut of light and color. The HDR imaging, referred to in some contexts as the 'new color-TV', approaches the latter problem by capturing multiple images of the same scene with different exposures and then composing them into a single image, spanning the whole dynamic range of

This work was supported by the Academy of Finland, project No. 213462 (Finnish Centre of Excellence program 2006-2011).
This paper extends the preliminary work of the authors first introduced in [Pirinen 07].

the scene [Mann 95], [Debevec 97]. The image composition step requires a preliminary calibration of the camera response [Debevec 97], [Mitsunaga 99]. A related problem then is to appropriately tone map the so-obtained HDR image back to a low-dynamic range (LDR) display. Tone mapping techniques range in complexity from a simple gamma-curve to sophisticated histogram equalization methods and complicated lightness perception models [Larson 97], [Devlin 02], [Krawczyk 05]. HDR techniques were reviewed in [Battiato 03].

State-of-the-art techniques for HDR imaging have been developed generically for the RGB color space. Luminance-chrominance color space representations have been neglected. However, HDR imaging techniques working in luminance-chrominance seem more meaningful and preferable for a number of reasons. *First*, decorrelated color spaces offer better compressibility. As a matter of fact, the near totality of image compression techniques store images in some luminance-chrominance space. When one starts with already-compressed multiple-exposure LDR images, it is more efficient to compose the HDR image directly in the same color space. The resulting HDR image is then better suited for compression and, if to be displayed, it can be mapped to sRGB during the tone mapping stage. *Second*, any HDR technique operating in RGB space requires post-composition white balancing since the three color channels undergo parallel transformations. While the white balancing would yield perceptually convincing colors, they might not be the true ones. For the sake of hue preservation and better compression, it is beneficial to opt for a luminance-chrominance space, even if the input data is in RGB, e.g. uncompressed TIFF. *Third*, the luminance channel, being a weighted average of the R, G, and B channels, enjoys a better signal-to-noise ratio (SNR), which is crucial if the HDR imaging process takes place in noisy conditions.

In this contribution, we address the problem of HDR imaging in a generic luminance-chrominance space, propose efficient algorithms for HDR image composition and tone mapping, and emphasize the benefits of such an approach. The paper is organized as follows. In Section 2 we provide a brief overview on the main properties of luminance-chrominance color spaces and introduce the notations used throughout the paper. HDR image composition, including camera response definition and processing the luminance and chrominance channels, is presented in Section 3. An adapted tone mapping method for luminance-chrominance HDR images is presented in Section 4. Examples demonstrating the viability of our approach are given in Section 5 and finally some conclusions are drawn in Section 6.

2. LUMINANCE-CHROMINANCE COLOR SPACES

We consider a generic luminance-chrominance color space linearly related to the RGB space. Loosely speaking, such a space is characterized by an achromatic luminance component, which corresponds to the grayscale part of the image, and two chrominance components, which are orthogonal to gray. Throughout the paper we use the following notations. We denote the luminance and the two chrominance channels by Y, U, and V, respectively. Let $\mathbf{z} = [z^R, z^G, z^B]$ be an image in the RGB space and $\boldsymbol{\zeta} = [\zeta^Y, \zeta^U, \zeta^V]$ be the same image in the luminance-chrominance space (we use Roman letters to denote images in RGB and the corresponding Greek letters to denote images in luminance-chrominance). Transformation of the image from RGB to luminance-chrominance is defined in matrix form as $\boldsymbol{\zeta} = \mathbf{z}\mathbf{A}$, where the matrix $\mathbf{A}$ is normalized in such a way that if $\mathbf{z}(\cdot) \in [0,1]^3$ then $\boldsymbol{\zeta}(\cdot) \in [0,1] \times [-0.5, 0.5]^2$. Because of this constraint, the first column of $\mathbf{A}$ has all elements positive, $a_{j,1} \geq 0$. We further assume that $\sum_{j=1}^{3} a_{j,1} = 1$, thus ensuring that the $[0,1]$ range of the luminance component is fully utilized. Example of such luminance-chrominance spaces are the "*opponent*" , the *YUV/YCbCr*, and the YIQ color spaces [Plataniotis 00]. The corresponding transformation matrices, for the "*opponent*" and the *YUV* color spaces respectively, are

$$\mathbf{A}_{opp} = \begin{bmatrix} \frac{1}{3} & \frac{1}{2} & \frac{1}{4} \\ \frac{1}{3} & 0 & \frac{-1}{2} \\ \frac{1}{3} & \frac{-1}{2} & \frac{1}{4} \end{bmatrix}, \quad \mathbf{A}_{yuv} = \begin{bmatrix} 0.30 & -0.17 & 0.50 \\ 0.59 & -0.33 & -0.42 \\ 0.11 & 0.50 & -0.08 \end{bmatrix}.$$

It can be noted, that the second and third columns of these matrices have all zero mean. This is equivalent to the inner product between the chrominance basis vectors and a vector corresponding to a gray pixel (for which $z^R = z^G = z^B$) always being zero. It means that gray is orthogonal to the chrominance components and that the inverse color transformation matrix $\mathbf{B} = \mathbf{A}^{-1}$ has the elements of its first row all equal, $b_{1,1} = b_{1,2} = b_{1,3}$. Since $\sum_{j=1}^{3} a_{j,1} b_{1,j} = 1$ and $\sum_{j=1}^{3} a_{j,1} = 1$, we obtain that $b_{1,1} = b_{1,2} = b_{1,3} = 1$. This means that the luminance component ζ^Y can be directly treated as a grayscale component of the RGB image $\mathbf{z}$, because the inverse transformation of the luminance component, $[\zeta^Y \; 0 \; 0]\, \mathbf{B} = \mathbf{z}_{\text{gray}}(\mathbf{x})$, is a grayscale image. We point out that these properties do not depend on the orthogonality of the matrix $\mathbf{A}$ (in fact the three columns of $\mathbf{A}_{yuv}$ are not orthogonal), but rather on the orthogonality between a constant vector and the second and third columns of the matrix.

The hue and saturation can be defined as $H = \arctan \frac{\zeta^U}{\zeta^V}$ and $S = \sqrt{(\zeta^U)^2 + (\zeta^V)^2}$, respectively. These can be

interpreted as the angular component and the length of a planar vector. Thus the triplet Y, H, and S corresponds to a luminance-chrominance representation with respect to cylindrical coordinates.

Luminance-chrominance transformations can be considered as special color decorrelating transforms. In particular, up to a diagonal normalization factor, the matrix $\mathbf{A}_{opp}$ is nothing but a 3×3 DCT transform matrix. Further, we note that the columns of $\mathbf{A}_{opp}$ are respectively a mean filter, a finite derivative filter, and a second derivative filter.

It is well known that natural color images exhibit a high correlation between the *R*, *G*, and *B* channels. Thus, it can be observed that *Y* contains most of the valuable information (edges, shades, objects, texture patterns, etc.) and *U* and *V* contain mostly low-frequency information (very often these channels come from undersampled data).

Luminance-chrominance transformations become particularly significant when the image $\mathbf{z}$ is corrupted by some independent noise. In fact, because of the typical correlation among z^R, z^G, z^B, one can observe that the luminance ζ^Y has noticeably higher signal-to-noise ratio (SNR) than the two chrominances ζ^U and ζ^V and than any of the individual RGB components z^R, z^G, z^B.

3. HDR IMAGE COMPOSITION

Consider a set of images $\boldsymbol{\zeta}_i = [\zeta_i^Y, \zeta_i^U, \zeta_i^V], i = 1, \ldots, N$ in a luminance-chrominance space, captured with different exposure times Δt_i and with LDR, assuming $\boldsymbol{\zeta}(\mathbf{x}) \in [0,1] \times [-0.5, 0.5]^2$, where $\mathbf{x} = [x_1, x_2]$ is a pixel coordinate. The goal is to obtain a single HDR image $\tilde{\boldsymbol{\zeta}} = \left[\tilde{\zeta}^Y, \tilde{\zeta}^U, \tilde{\zeta}^V\right]$ in the same color space. In our setting, the luminance and chrominance channels are treated separately. A pre-calibrated camera response function is used for the luminance channel, whereas a saturation-driven weighting is applied for the chrominance channels.

3.1. Camera response

Knowing the camera response is essential for determining the irradiance of the source scene from the given image data. With the pixel exposure $e(\mathbf{x})$ defined as the product between exposure time Δt and irradiance $E(\mathbf{x})$, $e(\mathbf{x}) = E(\mathbf{x})\,\Delta t$, the generic pixel output $\mathfrak{z}(\mathbf{x})$ is

$$\mathfrak{z}(\mathbf{x}) = f(e(\mathbf{x})) = f(E(\mathbf{x})\,\Delta t),$$

where f is the function describing the response of the output to the given exposure. Therefore, the irradiance can be obtained from the pixel output by the formal expression (see e.g. [Debevec 97])

$$\ln E(\mathbf{x}) = g(\mathfrak{z}(\mathbf{x})) - \ln \Delta t, \tag{1}$$

where $g = \ln f^{-1}$ is the (inverse) camera response function. This function can be estimated from a set of images of a fixed scene captured with different exposure times. Images for the calibration sequence are assumed to be perfectly aligned and shot under constant illumination. Noise should be negligible. For the camera response function calibration, a much larger set of images (i.e. a denser set of exposures) than typically available for the HDR composition, is used. The camera response function is estimated (calibrated) only once for each camera. The estimated function is then used for the linearization of the input values in all subsequent HDR compositions of the same device.

Conventionally, camera response functions are estimated separately for the R, G, and B channels, i.e. using these channels as the output $\mathfrak{z}$. There exist a number of techniques developed for this purpose, e.g., [Debevec 97], [Mitsunaga 99]. In our work, we estimate a single response function for the luminance channel only by replacing the output $\mathfrak{z}$ with ζ^Y. In practice, this can be done adapting any of the techniques developed for RGB data. Some specific modifications are however required in order to treat the luminance.

Because of underexposure (which produces dramatically low SNR) and overexposure (which results in clipping the values which would otherwise exceed the dynamic range) not all pixels from the given set of images can be used for the calibration of the camera response function. Additionally, only pixels having monotonically strictly increasing values between under- and overexposure, throughout the sequence, can be considered to be valid. Using these pixels, the function g can be fitted by minimizing the quadratic objective function [Debevec 97]

$$\sum_{j=1}^{P}\sum_{i=1}^{N} w_{\mathsf{cam}}(\zeta_i^Y(\mathbf{x}_j))\left[g(\zeta_i^Y(\mathbf{x}_j)) - \ln E_i - \ln \Delta t_i\right]^2 + \lambda \int_0^1 w_{\mathsf{cam}}(\zeta) g''(\zeta)^2 d\zeta, \tag{2}$$

where P is the number of pixels used from each image and w_{cam} is a weight function limiting the effect of the under- and overexposed pixels. The regularization term on the right-hand side uses a penalty on the second derivative of g to ensure the smoothness of the solution. We prefer to use a relatively high pixel count (e.g. 1000 pixels) in order to minimize the need for regularization in the data fitting. We solve the system of equations employing singular-value decomposition, in a fashion

similar to that of [Debevec 97]. Since we work with the luminances ζ_i^Y, we do not process directly the sensor output, but only a combination of its components. This combination can include overexposed components without reaching the upper limit of its dynamic range. Such pixels have to be penalized in the processing. To ensure a more powerful attenuation of the possibly overexposed pixels, instead of a simple triangular hat function (e.g. as in [Debevec 97]) we use an asymmetric function of the form $w_{\mathsf{cam}}(\rho) = \rho^{\alpha}(1-\rho)^{\beta}$ where $0 \leq \rho \leq 1$ and $1 \leq \alpha < \beta$. The latter inequality between α and β ensures the asymmetry of the weight function and especially the faster decay of the weights for the higher end of the intensity range. An example of such a weight function is given in Figure 1 for $\alpha = 1$ and $\beta = 6$. An example of a camera response function for the luminance solved with this method is illustrated in Figure 2. When looking at the camera response one can observe an abrupt peak towards the right end of the plot. This is a result of the clipping of the overexposed pixels. It becomes evident that such pixels cannot be directly included in the subsequent composition step. Instead they have to be penalized with weights.

We wish to emphasize that the issue of overexposure being present also in pixels whose value is lower than the maximum is not absent even for the conventional approaches dealing in the RGB space. *First*, the R, G, and B channels in the images which are used in the calibration never coincide with the original RGB components of the sensor (this is the actual element limiting the dynamic range in most camera systems). In fact, several intermediate processing stages (which include color matrixing, Bayer pattern color interpolation, white balance, etc.) are typically present. These operations combine the original RGB components of the raw-data and can thus introduce clipped (overexposed) components into pixels whose final output value is still lower than the maximum. *Second*, if the data has been precedently compressed (e.g. JPEG), the found values might not exactly coincide with the original (uncompressed) ones. *Finally*, let us note that even in the RAW data some correlation between adjacent pixels in the same rows of the CMOS/CCD sensor is introduced during the read-out process. Especially in the case of overexposure, also blooming can be present. Therefore, processing luminance data does not introduce any fundamental complication to the value or meaning of the camera-response function. By using a properly selected weight function we can effectively deal with the wider overexposure region at the end of the dynamic range. Additionally, since the luminance channel always benefits from an increased SNR when compared with the R,G,B channels, the procedure for the luminance channel is less sensitive to noise than the corresponding ones in RGB space.

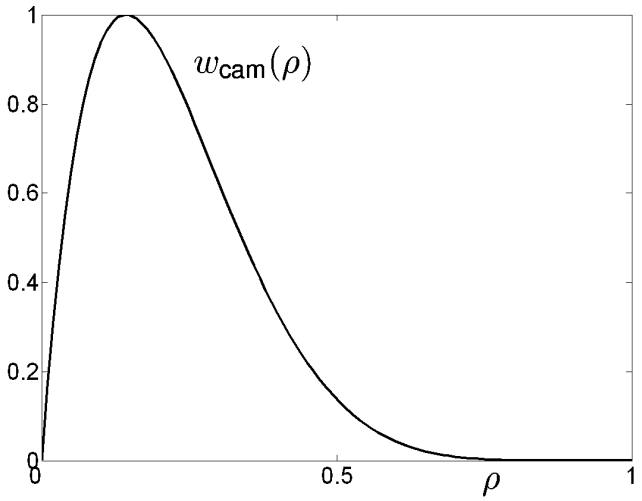

Fig. 1. Camera response calibration weight function $w_{cam}(\rho) = \rho^{\alpha}(1-\rho)^{\beta}$, where $\alpha = 1$, $\beta = 6$. The function has been normalized with respect to its maximum.

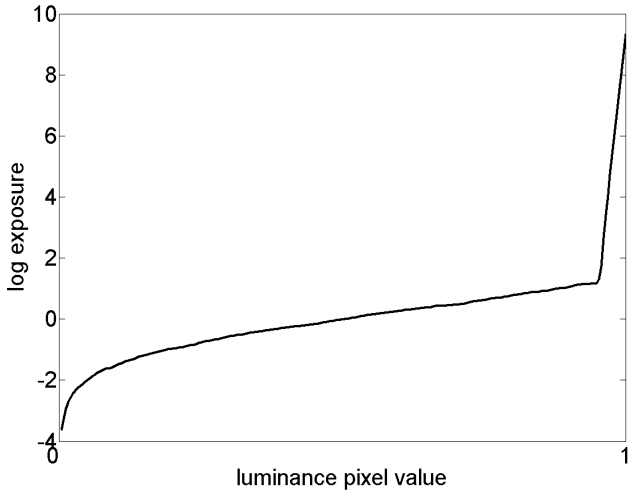

Fig. 2. Estimated inverse response function g for luminance channel of Nikon COOLPIX E4500.

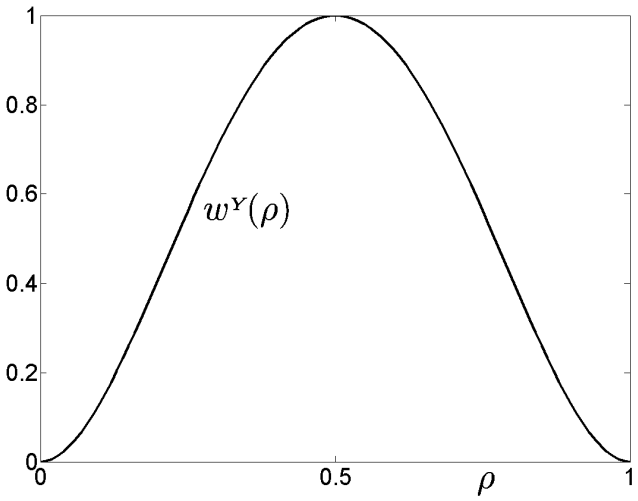

Fig. 3. Luminance channel composition weight function $w^Y(\rho) = \rho^\alpha(1-\rho)^\beta$, where $\alpha = 2$, $\beta = 2$. The function has been normalized with respect to its maximum.

3.2. Luminance component composition

We obtain the HDR luminance component by a pixel-wise weighted average of the pixel log irradiances defined according to Eq. (1) as $\ln E_i(\mathbf{x}) = g(\zeta_i^Y(\mathbf{x})) - \ln \Delta t_i$. As observed in the previous section, pixels whose value is close to 0 or 1, carry little valuable information, respectively because of low SNR (underexposure) and clipping (overexposure). Therefore, these pixels are penalized employing weights during the composition. As a weighting function we use a polynomial function $w^Y(\rho) = \rho^\alpha(1-\rho)^\beta$, where $0 \leq \rho \leq 1$ and $\alpha = 2$, $\beta = 2$ thus ensuring a smaller impact of the under- or overexposed pixels. An example of such a weight function for the luminance is given in Figure 3. The logarithmic HDR luminance is obtained as

$$\ln \tilde{\zeta}^Y(\mathbf{x}) = \frac{\sum_{i=1}^N w^Y(\zeta_i^Y(\mathbf{x}))(g(\zeta_i^Y(\mathbf{x})) - \ln \Delta t_i)}{\sum_{i=1}^N w^Y(\zeta_i^Y(\mathbf{x}))}. \tag{3}$$

Because of the nature of the camera response function g, the HDR luminance is obtained in logarithmic scale. After employing the natural exponential, the resulting values are positive, ranging within $[10^{-4}\ 10^4]$. Within this range a single HDR luminance image can have a dynamic range of up to 5 log units.

3.3. Chrominance components composition

For the chrominance components we define no camera response. Instead, we weight the chrominances in relation to the level of color saturation. The higher the color saturation, the more the pixel contains valuable chromatic information, and thus the

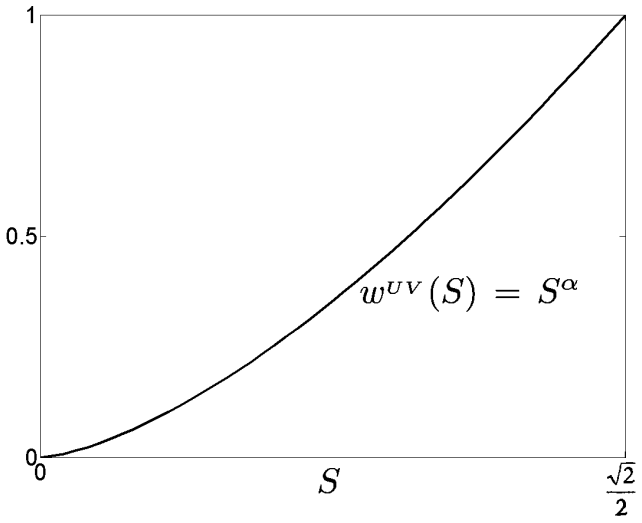

Fig. 4. Chrominance composition weight function $w^{UV}(S) = S^{\alpha}$, where $\alpha = 1.5$. The function has been normalized with respect to its maximum and .

higher the weight. This is motivated by the fact that when a pixel is over- or underexposed it is always less saturated than it would be at the correct exposure. More specifically, $w^{UV}(S) = S^{\alpha}$, where $\alpha > 1$. In our experiments, we have found that $\alpha = 1.5$ is a good choice. A saturation-based chrominance weight function is illustrated in Figure 4. To guarantee the color preservation, we use the same weights for both chromatic components and compose any chromatic component $C \in \{U, V\}$ as

$$\tilde{\zeta}^{C}(\mathbf{x}) = \frac{\sum_{i=1}^{N} w^{UV}(S_i(\mathbf{x}))\zeta_i^{C}(\mathbf{x})}{\sum_{i=1}^{N} w^{UV}(S_i(\mathbf{x}))}, \tag{4}$$

where S_i denotes the saturation of $\boldsymbol{\zeta}_i$. We point out that being a convex combination of the input chrominances, the range of $\tilde{\zeta}^{C}(\mathbf{x})$ is again in $[-0.5, 0.5]$. However, because of averaging, the possible number of distinct chrominance values is remarkably higher than in the original source sequence.

Another intuitively interesting approach would be to use the luminance-dependent weights w^{Y} for not only the luminance but also for the chrominance channels. Loosely this approach would be similar to the proposed saturation-driven weighting because of the fact that color saturation typically decreases with the luminance moving closer to the extremes. However, in our experiments we have found that saturation-based weighting provides a better reproduction of color especially for saturated highly exposed or low-lit details.

3.3.1. HDR saturation control

If the composed HDR image is to be displayed or processed on an HDR system with RGB input, the following approach can be used in order to reproduce colors with a saturation faithful to the original scene. As stated in Section 3.2, the value range of the luminance channel after the composition is roughly up to 5 log units whereas the HDR chrominance is a denser sampling of the [-0.5 0.5] interval. If the luminance-chrominance HDR image is to be opened on a device or application with RGB input, the chrominances need to match the range of the luminance in order to produce a meaningful RGB HDR image. To this purpose we have developed this *saturation control* which approximates the chrominance scaling needed to match the range of the luminance.

Let us define the scalar proportionality factor $\mu(\mathbf{x})$ between the HDR luminance $\tilde{\zeta}^Y$ and the weighted average of the LDR luminances $\zeta_i^Y(\mathbf{x})$ with weights $w^{UV}(S_i(\mathbf{x}))$ as

$$\mu(\mathbf{x}) = \frac{\tilde{\zeta}^Y \sum_{i=1}^{N} w^{UV}(S_i(\mathbf{x}))}{\sum_{i=1}^{N} w^{UV}(S_i(\mathbf{x}))\,\zeta_i^Y(\mathbf{x})}. \tag{5}$$

Then, the HDR image in RGB space is obtained by the normalized inverse color transformation

$$\tilde{\mathbf{z}}(\mathbf{x}) = \tilde{\boldsymbol{\zeta}}(\mathbf{x}) \begin{bmatrix} 1 & 0 & 0 \\ 0 & \mu(\mathbf{x}) & 0 \\ 0 & 0 & \mu(\mathbf{x}) \end{bmatrix} \mathbf{B}.$$

Here the normalization is realized by multiplication against the diagonal matrix $diag(1, \mu(\mathbf{x}), \mu(\mathbf{x}))$ which scales the two chrominances $\tilde{\zeta}^U$ and $\tilde{\zeta}^V$ yielding a value of saturation which matches the full dynamic range achieved by $\tilde{\zeta}^Y$. Indeed, the weights $w^{UV}(S_i(\mathbf{x}))$ in Eq. (5) and Eq. (4) are exactly the same. Observe that the value of $\mu(\mathbf{x})$ does not have any influence on the hue nor on the luminance of $\tilde{\mathbf{z}}(\mathbf{x})$, but controls only its saturation.

4. TONE MAPPING FOR LUMINANCE-CHROMINANCE HDR IMAGES

Tone mapping is an HDR imaging technique used to approximate the visibility of the tones of an HDR image on an LDR media, such as LCD and CRT displays or print-outs [Reinhard 06]. Essentially, tone mapping compresses the global contrast of a scene to fit into the displayable range of a media while preserving details and color. In this paper we consider only global

tone mapping techniques.

In this section we present a method for tone mapping luminance-chrominance HDR images acquired with the technique described in Section 3. We give the means for applying existing tone mapping operators for the luminance channel and complement the luminance mapping with a novel approach for the chromatic data.

A number of tone mapping methods developed for RGB HDR images exist. As the tone mapping procedure is by definition based on the compression of luminance, these techniques can easily be adapted for the luminance (gray-scale) range reduction. We denote such a luminance range reduction operator as $\mathcal{T}$. Its output is a luminance image with range $[0,1]$, i.e. $\mathcal{T}\left(\tilde{\zeta}^{Y}\right)(\cdot) \in [0,1]$. As for the chromatic channels, we suggest a simple, yet effective approach.

The sRGB gamut does not allow the rendition of very dark or very bright vivid and saturated colors which exist in real scenes and which are captured in HDR images. Therefore there exists a need for chromatic tone mapping. In our approach, in order to get faithful colors that fit into the sRGB gamut we keep the hue intact while sacrificing saturation. Introducing a scaling factor δ for the two chrominances will then not change the hue, but will scale down the saturation. The scheme we use to guarantee legal sRGB values is embedded in the color space transformation itself and described as follows.

Let $\mathbf{B} = \mathbf{A}^{-1}$ be the luminance-chrominance to RGB transformation matrix and define the gray (achromatic) image and its chromatic complement image in RGB space by

$$\mathring{\mathbf{z}}_{\text{gray}}(\mathbf{x}) = \left[\mathring{z}^{R}_{\text{gray}}(\mathbf{x})\ \ \mathring{z}^{G}_{\text{gray}}(\mathbf{x})\ \ \mathring{z}^{B}_{\text{gray}}(\mathbf{x})\right] = \begin{bmatrix} \mathcal{T}\left(\tilde{\zeta}^{Y}\right)(\mathbf{x}) \\ 0 \\ 0 \end{bmatrix}^{T} \mathbf{B},$$

$$\mathbf{z}_{\text{chrom}}(\mathbf{x}) = \left[z^{R}_{\text{chrom}}(\mathbf{x})\ \ z^{G}_{\text{chrom}}(\mathbf{x})\ \ z^{B}_{\text{chrom}}(\mathbf{x})\right] = \begin{bmatrix} 0 \\ \tilde{\zeta}^{U}(\mathbf{x}) \\ \tilde{\zeta}^{V}(\mathbf{x}) \end{bmatrix}^{T} \mathbf{B}.$$

We remark that $\mathring{\mathbf{z}}_{\text{gray}}(\mathbf{x})$ is truly a gray image because in RGB to luminance-chrominance transforms $b_{1,1} = b_{1,2} = b_{1,3}$. We look for a map $\delta \geq 0$ such that

$$\mathring{\mathbf{z}}(\mathbf{x}) = \mathring{\mathbf{z}}_{\text{gray}}(\mathbf{x}) + \delta(\mathbf{x})\,\mathbf{z}_{\text{chrom}}(\mathbf{x}) \in [0,1]^{3}. \tag{6}$$

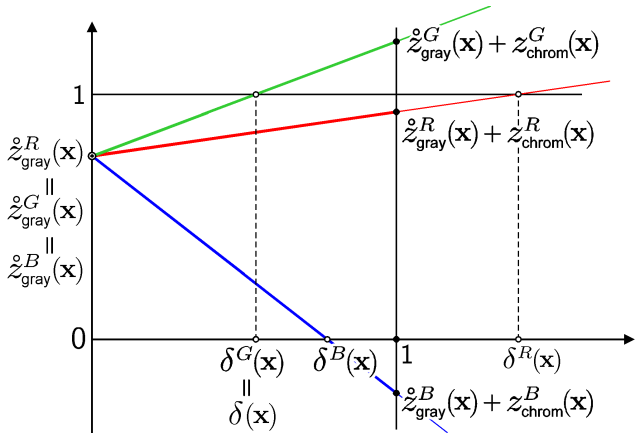

Fig. 5. Illustration of the definition of the chromatic tone mapping parameter δ.

We can define it by $\delta(\mathbf{x}) = \min\{1, \delta^R(\mathbf{x}), \delta^G(\mathbf{x}), \delta^B(\mathbf{x})\}$ where

$$\delta^R(\mathbf{x}) = \begin{cases} \frac{\mathring{z}^R_{\text{gray}}(\mathbf{x})}{-z^R_{\text{chrom}}(\mathbf{x})} & \text{if } z^R_{\text{chrom}}(\mathbf{x}) < 0 \\ \frac{1-\mathring{z}^R_{\text{gray}}(\mathbf{x})}{z^R_{\text{chrom}}(\mathbf{x})} & \text{if } z^R_{\text{chrom}}(\mathbf{x}) > 0 \\ 1 & \text{if } z^R_{\text{chrom}}(\mathbf{x}) = 0 \end{cases}$$

and δ^G and δ^B are defined analogously. Thus, $\delta(\mathbf{x})$ is the largest scalar smaller or equal to one, which allows the condition (6) to hold. Figure 5 illustrates the definition of $\delta(\mathbf{x})$. From the figure it is easy to realize that the hue, i.e. the angle of the vector, of $\mathring{\mathbf{z}}(\mathbf{x})$ is not influenced by δ, whereas the saturation is scaled proportionally to it. Roughly speaking, the low dynamic range image $\mathring{\mathbf{z}}(\mathbf{x})$ has colors which have the same hue as those in the HDR image $\tilde{\boldsymbol{\zeta}}$ and which are desaturated as little as is needed to fit within the sRGB gamut.

It is now obvious that the tone mapped LDR image can be defined in luminance-chrominance space as

$$\mathring{\boldsymbol{\zeta}}(\mathbf{x}) = \left[\mathcal{T}\left(\tilde{\zeta}^Y\right)(\mathbf{x}) \quad \delta(\mathbf{x})\,\tilde{\zeta}^U(\mathbf{x}) \quad \delta(\mathbf{x})\,\tilde{\zeta}^V(\mathbf{x})\right].$$

The tone mapped luminance-chrominance image $\mathring{\boldsymbol{\zeta}}$ can be compressed and stored directly with an arbitrary method (for example, DCT-based compression, as in JPEG), and for display transformed into RGB using the matrix $\mathbf{B}$. We demonstrate that this approach yields lively, realistic colors.

5. RESULTS

We compare the proposed HDR imaging approach in luminance-chrominance space against established techniques working in the RGB space. We consider two cases: the case of noise-free LDR images and the case of LDR images corrupted by a certain amount of noise. We emphasize that the focus in visual evaluation of the methods should be in the perception of hue, rather than brightness which is strongly affected by the selection of a tone mapping operator.

5.1. Noise-free case

A sequence shot with the lowest possible ISO for a given camera is in this context considered to be noise-free. We show experiments with two sets of images. The first set, $\{\mathbf{z}_i\}_{i=1,2,3}$ was captured with Fujifilm FinePix S5600 with exposure times (seconds) $\{1/5, 1/20, 1/80\}$ (Figure 6) and ISO 64. The second set, $\{\mathbf{z}_i\}_{i=1,2,3,4,5}$ was captured with Nikon COOLPIX E4500 with exposure times $\{1/4, 1/15, 1/60, 1/250, 1/1000\}$ and ISO 100 (Figure 9). Using these two sets, HDR images have been composed both in RGB and luminance-chrominance space. The HDR images have been then tone-mapped back to LDR ones for display. Debevec's HDR Shop v.1.0.3 software [HDRShop] has been used for the HDR composition in RGB space.

There are a number of tone mapping techniques, most of them requiring careful tuning of a set of input parameters. For the RGB HDR tone mapping we have opted for the *photographic tone reproduction operator* [Reinhard 06] as it is a global tone mapping technique with fully automatic parameter estimation. The tone mapped result of processing the sequences in RGB space are shown in Figures 7 and 10. In our approach, we first transform the sequences to the opponent color space. Then, we perform the HDR image composition as described in Section 3. The so-obtained HDR image is tone mapped according to the method described in Section 4. The operator $\mathcal{T}$ used for reducing the range of $\tilde{\zeta}^Y$ is an adaptation of the histogram adjustment technique developed in [Larson 97]. For $\mathcal{T}$, only the case of a simple linear ceiling is implemented. Also no display dependent parameters are defined; instead the resulting image is scaled to the standard 8-bit output of normalized range [0,1]. Thus, $\mathcal{T}$ is a very simple and fully automatic luminance range reduction operator with no parameter adjustment whatsoever, motivating the comparison to an equivalently automatic tone mapping operator in RGB space.

Our result for the sequences are shown in Figures 8 and 11. Beside some obvious differences in brightness, chromatic distortions which can arise from the RGB processing can be seen when the tone-mapped images are compared with the source

[1] All images used to produce the examples presented in this paper are made available in the project website `http://www.cs.tut.fi/~hdr/`.

sequences in Figures 6 and 9. The RGB approach seems to systematically fail in reproducing colors at the dark end of the dynamic range of the scene. This is best pronounced at the colorchart cover at the foreground of Figures 9, 10, and 11, and at the wall under the table on the left hand side of the same figures. In the same areas, the luminance-chrominance approach produces lively colors, faithful to the original ones. These results are further illustrated in the enlarged details of the above-mentioned parts, shown in Figures 12 and 13. The detail figures contain, starting from left, the frame of the original sequence which is correctly exposed for the detail in question, the tone mapped RGB HDR image, and the luminance-chrominance HDR image composed and tone mapped according to the procedure described in this paper. Overall, the colors obtained by processing in luminance-chrominance space are much more faithful, as the hue has been preserved.

5.2. Noisy case

A further notable advantage of our approach appears when the source sequence is degraded by noise. We present three different types of results for noisy data. First, we give a visual assessment of HDR images corrupted with artificial noise. Then, we do the same for images shot with a very high ISO setting, thus visibly corrupted by noise from the camera digital imaging sensor. Third, we compare numerically the noise attenuation properties of processing in RGB against processing in two separate luminance-chrominance spaces.

5.2.1. Artificial noise

In our simulations we added zero-mean Gaussian noise with standard-deviations $\sigma = \frac{5}{255}$, $\frac{15}{255}$, and $\frac{25}{255}$ to the second set of source LDR images (Figure 9), and composed an HDR image with the approach described in this paper as well as with the RGB approach of Debevec's HDR Shop [HDRShop]. Scanlines of the noisy HDR images ($\sigma = \frac{15}{255}$) imposed on the scanlines of the noise-free references can be seen in Figure 15 (RGB) and in Figure 17 (luminance-chrominance). The difference in noise levels can also be seen in the tone mapped images, given in Figure 14 (RGB) and Figure 16 (luminance-chrominance). The luminance-chrominance approach preserves details fairly well in many parts where the RGB approach completely fails. For example, details of the colorchart cover in the foreground are completely lost with the RGB approach whereas our method preserves the visibility much better.

5.2.2. *Real noise*

We also shot a sequence with the Nikon COOLPIX E4500 with ISO 800 to acquire a source sequence that was inherently noisy. Because for the given camera, the native (lowest) ISO is 100, by increasing the ISO up to 800 we end up boosting not only the signal, but also the noise, which becomes very noticeable in most parts of the image. For this sequence we show two details; one from the darker part (Figure 18) and one from the lighter (Figure 19). From the detail sequences the presence of the blue noise can be distinguished especially in the darker frames. The notable noise amplification of the RGB approach is a consequence of the separate weighting of the three channels. As the noise is most visible in the blue channel in the dark parts of the image, it is boosted out of proportion by the weighting. Instead, the luminance channel is much less vulnerable to noise and the exaggerated blue noise of the tone mapped Figure 20 done by processing in RGB cannot be seen in the luminance-chrominance processing counterpart of Figure 21.

Differing from the other tone mapped results shown in the paper, the tone mapping of both noisy images shown in Figures 20 and 21 for RGB and luminance chrominance composition respectively, was done under HDR Shop with the included plugin, implementing the photographic tone reproduction operator introduced in [Reinhard 02]. Default settings were used, except for sharpening and gamma correction, which were not done in the tone mapping process. For the purpose of correctly transforming a luminance-chrominance HDR image into RGB space, the saturation control described in Section 3.3.1 was performed on the image before the standard color space transformation realized by multiplication against the matrix $\mathbf{B} = \mathbf{A}_{opp}^{-1}$.

5.2.3. *Objective noise evaluation*

Because of the nonlinear nature of HDR processing, the addition of a zero-mean noise to the source sequence $\{\mathbf{z}_i\}_{i=1}^{N}$ does not generally result in the introduction of simple zero-mean errors in the composed HDR image $\{\tilde{\mathbf{z}}_i\}_{i=1}^{N}$ or in the tone mapped image $\{\mathring{\mathbf{z}}_i\}_{i=1}^{N}$. Strictly speaking, the mathematical expectation of the image composed from the noisy sequence does not coincide with the image composed from the noise-free sequence. A number of alterations might be present in the underlying signal, such as different scaling due to the wider histogram of the noisy data and shifts in the intensities of darker and brighter areas caused by the asymmetric distribution of the clipped noise. These make it difficult to quantitatively measure the degradation due to noise using reference-based error criteria such as the MSE, PSNR, etc. It should be observed that most of these alterations are not necessarily negative (e.g., the different scaling of the data is absolutely negligible).

In order to quantify the effect of noise presence, or the "noisiness", of the HDR images composed from noisy source sequences, we resort to a *non-reference-based* criterion. In particular, we use a normalized robust estimator of the standard-deviation (*NRSTD*) of the noise defined as

$$\textit{NRSTD}\,(\xi) = \frac{median\,\{|\xi \circledast \mathcal{H}|\}}{0.6745}\,\frac{1}{\max\{\xi \circledast \mathcal{L}\} - \min\{\xi \circledast \mathcal{L}\}}, \tag{7}$$

where ξ is the degraded "noisy" image, $\circledast$ denotes the convolution, and $\mathcal{H}$ and $\mathcal{L}$ are a high-pass and a low-pass filtering kernel, respectively, satisfying

$$\int \mathcal{H} = 0, \quad \int \mathcal{H}^2 = 1, \text{ and } \int \mathcal{L} = 1.$$

We choose $\mathcal{H} = \psi^T\psi$, with $\psi = [0.035\ \ 0.085\ \ -0.135\ \ -0.460\ 0.807\ \ -0.333]$ (a Daubechies wavelet), and $\mathcal{L}$ to be a 7×7 uniform kernel equal to $\frac{1}{49}$. The factor on the left in Eq. (7) is essentially the classic robust estimator of the noise standard deviation [Donoho 94] given as the median of the wavelet detail coefficients' moduli at the finest scale. It assumes that the image is concentrated at the coarser scales and that the finest scale contains mostly noise. The denominator in the right factor of Eq. (7) serves to normalize the estimated standard-deviation with respect to the dynamic range of a smoothed version of ξ, in which the effects of the noise have been substantially suppressed.

With the intention of obtaining meaningful and comparable results, we calculate the NRSTD on the luminance component of the HDR images only. This is based on the fact that the image content is differently distributed among the three channels of different color-space representations and the luminance is the most informative one. For the RGB HDR images this component is simply the average of the R, G, and B channels. The results are given in Tables 1 and 2. As can be seen

σ	$NRSTD_{RGB}$	$NRSTD_{opponent}$	$NRSTD_{yuv}$
0/255	$8.76 \cdot 10^{-5}$	$12.3 \cdot 10^{-5}$	$10.5 \cdot 10^{-5}$
5/255	$3.15 \cdot 10^{-4}$	$2.26 \cdot 10^{-4}$	$2.45 \cdot 10^{-4}$
15/255	$3.83 \cdot 10^{-3}$	$0.97 \cdot 10^{-3}$	$1.24 \cdot 10^{-3}$
25/255	$1.20 \cdot 10^{-2}$	$0.30 \cdot 10^{-2}$	$0.39 \cdot 10^{-2}$

Table 1. NRSTD values calculated on the luminance channel of the HDR images acquired with the RGB and luminance-chrominance approaches in opponent and in *YUV* color space respectively. The case of $\sigma = 0/255$ is shown as a reference.

from the tables, for both various levels of artificial noise as well as real noise present in the original sequence, the described approach in luminance-chrominance space produces HDR images with substantially lower noise standard deviation. The objective noise standard deviation estimations of Tables 1 and 2 reinforce the visual impression given by all of the shown

examples (Figures 14, 15, 16, 17, 20 and 21): the HDR luminance composed according to Eq. (3) is much less noisy than the one composed following the conventional RGB procedures.

One might wonder why it is so. After all, the luminance calculated as the average of the three HDR R,G,B channels is also much less noisy than each of these channels. The dramatic difference between the two sets of results can be explained by considering the weights used in the composition. These weights are the crucial element on which all the HDR composition depends. In the RGB approach, channels are processed separately. It means that the weights used for composing, say, the HDR red channel $\tilde{z}^R$ are based on the noisy LDR z_i^R, $i = 1, \ldots, N$, channels only. In our approach, the weights are instead defined as functions of the luminance components ζ_i^Y, $i = 1, \ldots, N$, which have about only half of the standard-deviation of the individual components z_i^C, $c = R, G, B$, $i = 1, \ldots, N$. Thus, our weights are less affected by the noise than their counterpart in the RGB processing.

From Tables 1 and 2 one can note a slight difference between the opponent and the *YUV* color spaces. The fact that this difference is always in favor of the opponent color space can be explained by observing that the opponent color space is among the most efficient ones when considering solely denoising properties. This is because of the orthogonality between the columns of A_{opp} as well as because the first column has the minimum ℓ^2 norm among the ones satisfying the condition $\sum_{j=1}^{3} a_{j,1} = 1$. It is pointed out however that the difference between opponent and other luminance-chrominance color spaces is marginal when compared to the difference with processing in RGB, and the selection of color space should be motivated by the format of the data rather than any single property of any given color space.

6. CONCLUSIONS

In this contribution we have presented an efficient method for composing HDR images in luminance-chrominance color spaces along with a method for tone mapping images acquired in this fashion. Compared to the conventional RGB approach, the described approach produces HDR images superior in color preservation and noise attenuation. The noise resilience of the proposed approach appears especially practical if the data is subject to some further postprocessing such as sharpening. This

$NRSTD_{RGB}$	$NRSTD_{opponent}$	$NRSTD_{yuv}$
$2.99 \cdot 10^{-4}$	$0.79 \cdot 10^{-4}$	$0.87 \cdot 10^{-4}$

Table 2. NRSTD values calculated on the luminance channel of the HDR images acquired with the RGB and luminance-chrominance approaches in opponent and in *YUV* color space respectively. Sequence with real noise from the camera sensor, shot with ISO 800.

Fig. 6. Three-image source sequence used to compose the HDR images.

Fig. 7. HDR image composed and tone mapped by processing in RGB color space.

operation is implemented in consumer cameras, partly to overcome limitations of the optical system of the camera, partly to provide the user with a more attractive photographic result (though maybe very different than the reality). It is well known that sharpening, by boosting the high-frequencies, amplifies the noise. The higher SNR of the luminance ensures that the image can be sharpened without introducing disturbing noise or artifacts. Additionally, the human visual system lacks good sensitivity to high-frequencies in the chrominances. Thus, sharpening is mostly needed for the luminance.

We have presented our results for HDR images composed in the opponent color space. The differences caused by the selection of color space are almost always perceptual and subjective rather than objective. For all the luminance-chrominance color spaces falling under the umbrella defined in Section 2 the same properties hold for noise attenuation and hue preservation. Thus, the results are not presented here to avoid duplication. Generally our approach yields more realistic colors with better noise suppression qualities compared to the traditional RGB methods, and does so in a computationally efficient manner. Objective comparison of computational efficiency is difficult due to, among others, differences in implementation

Fig. 8. HDR image composed and tone mapped by our approach in luminance-chrominance space.

Fig. 9. Five-image source sequence used to compose the HDR images.

and execution environments and optimization of the different methods. However, in terms of complexity, the presented approach is not less efficient than any RGB-based one. In particular, the complexity of the proposed luminance-chrominance image composition is comparable to that of [Debevec 97], which is arguably the simplest composition method in the literature. Likewise, the proposed luminance-chrominance tone mapping technique is comparable to performing the selected tone mapping operator $\mathcal{T}$ on a single channel (monochromatic image). Moreover, if starting with previously compressed luminance-chrominance images (e.g. JPEG), the conversions from and to RGB are not necessary, further simplifying the application of our methods. It is our belief that the advantages of the proposed approach shall motivate the migration of HDR processing from RGB to luminance-chrominance space.

Fig. 10. HDR image composed and tone mapped by processing in RGB color space.

7. REFERENCES

[Battiato 03] S. Battiato, A. Castorina & M. Mancuso. *High dynamic range imaging for digital still camera: an overview*. Journal of Electronic Imaging, vol. 12, pages 459–469, jul 2003.

[Debevec 97] P. Debevec & J. Malik. *Recovering high dynamic range radiance maps from photographs*. In Proc. 24th Conf. Comp. Graphics and Interactive Techniques, pages 369–378, 1997.

[Devlin 02] K. Devlin, A. Chalmers, A. Wilkie & W. Purgathofer. *Tone reproduction and physically based spectral rendering*. In Proc. EUROGRAPHICS'02, volume 22, 2002.

[Donoho 94] D.L. Donoho & I.M. Johnstone. *Ideal spatial adaptation via wavelet shrinkage*. Biometrika, vol. 81, no. 3, pages 425–455, 1994.

[HDRShop] HDRShop. High dynamic range image processing and manipulation. available at http://www.hdrshop.com.

Fig. 11. HDR image composed and tone mapped by our approach in luminance-chrominance space.

[Krawczyk 05] G. Krawczyk, K. Myszkowski & H. Seidel. *Lightness Perception in Tone Reproduction for High Dynamic Range Images*. In Proc. EUROGRAPHICS'05, volume 24, 2005.

[Larson 97] G.W. Larson, H. Rushmeier & C. Piatko. *A Visibility Matching Tone Reproduction Operator for High Dynamic Range Scenes*. IEEE Trans. Visual and Computer Graphics, vol. 3, no. 4, pages 291–306, 1997.

[Mann 95] S. Mann & R. Picard. *Being 'undigital' with digital cameras: Extending Dynamic Range by Combining Differently Exposed Pictures*. In Proc. IS&T 46th Conf., pages 422–428, 1995.

[Mitsunaga 99] T. Mitsunaga & S.K. Nayar. *Radiometric Self Calibration*. In Proc. IEEE Conf. Comp. Vision and Pattern Recognition, volume 2, pages 374–380, 1999.

[Pirinen 07] O. Pirinen, A. Foi & A. Gotchev. *High Dynamic Range (HDR) Imaging in Luminance-Chrominance Space*. In Proc. of the Third International Workshop on Video Processing and Quality Metrics for Consumer Electronics, 2007.

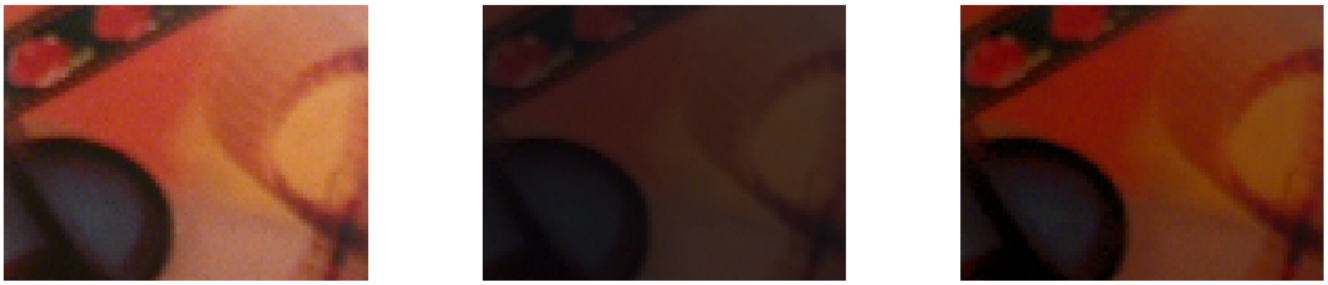

Fig. 12. An enlarged detail illustrating the color preservation of our method. The images are from left to right as follows: Exposure with best color and detail from the original sequence. Tone mapped RGB HDR image. Tone mapped luminance-chrominance HDR image.

Fig. 13. Another enlarged detail illustrating the color preservation properties of our method. The images are from left to right as follows: Exposure with best color and detail from the original sequence. Tone mapped RGB HDR image. Tone mapped luminance-chrominance HDR image.

[Plataniotis 00] K. Plataniotis & A. Venetsanopoulos. Color image processing and applications. Springer-Verlag New York, Inc., New York, NY, 2000.

[Reinhard 02] E. Reinhard, M. Stark, P. Shirley & J. Ferwerda. *Photographic tone reproduction for digital images*. In Proceedings of ACM SIGGRAPH 2002, 2002.

[Reinhard 06] E. Reinhard, G. Ward, S. Pattanaik & P. Debevec. High dynamic range imaging. Morgan Kaufmann Publishers, San Francisco, CA, 2006.

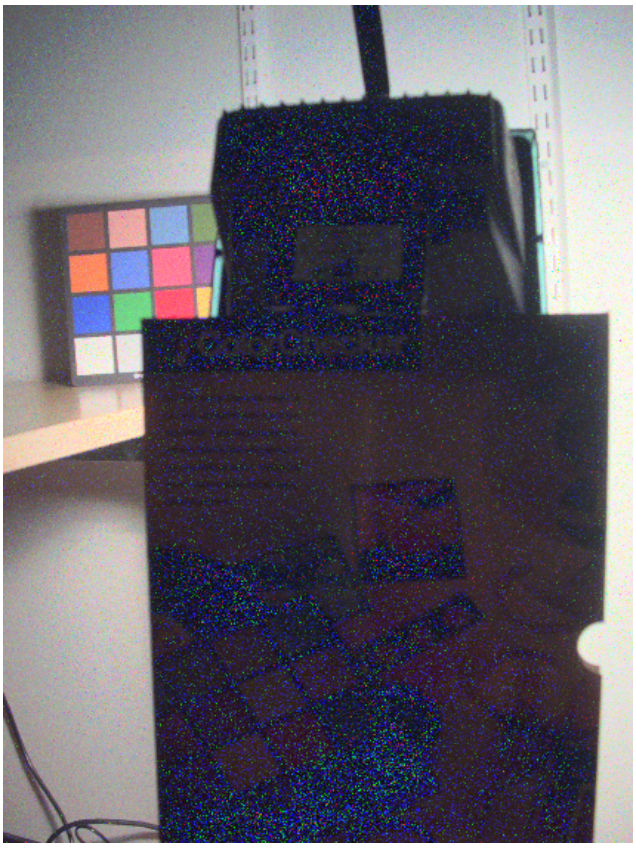

Fig. 14. HDR image composed and tone mapped from the noisy ($\sigma^2 = \frac{15}{255}$) sequence in RGB color space.

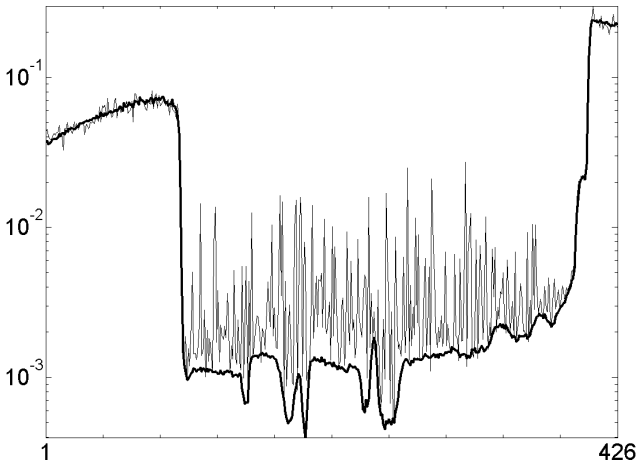

Fig. 15. Horizontal scanline (450) comparison between the noise-free (shown tone mapped in Figure 10) and the noisy (shown tone mapped in Figure 14) HDR images processed in RGB space ($\sigma = \frac{15}{255}$).

Fig. 16. HDR image composed and tone mapped from the noisy ($\sigma^2 = \frac{15}{255}$) sequence by our approach in luminance-chrominance space.

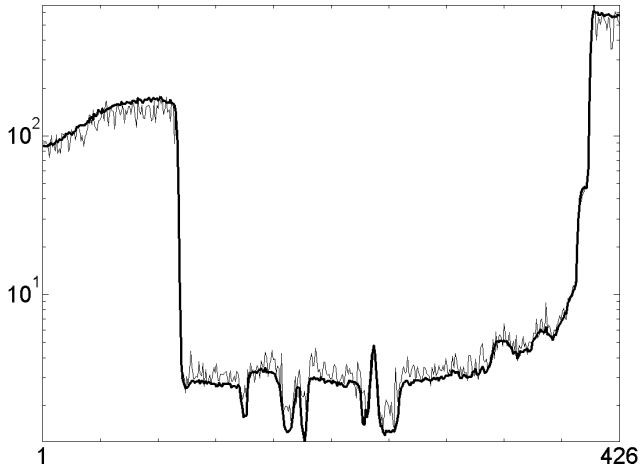

Fig. 17. Horizontal scanline (450) comparison between the noise-free (shown tone mapped in Figure 11) and the noisy (shown tone mapped in Figure 16) HDR images processed by our approach in luminance-chrominance space ($\sigma = \frac{15}{255}$).

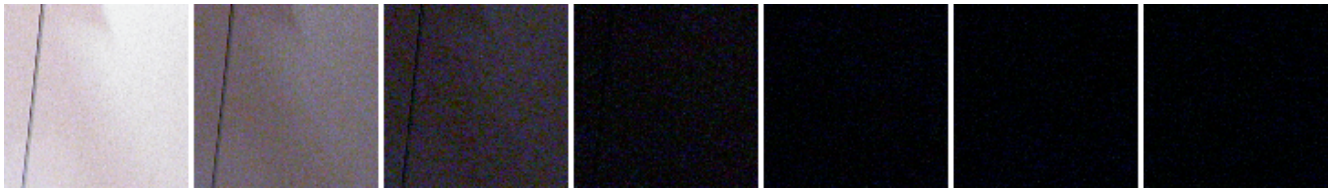

Fig. 18. A clipped detail of the darker part of the seven-frame noisy sequence shot with ISO 800. The blue noise enhanced by the RGB approach can be seen in the darker frames.

Fig. 19. A clipped detail of the lighter part of the seven-frame noisy sequence shot with ISO 800. The blue noise enhanced by the RGB approach can be seen in the darker frames.

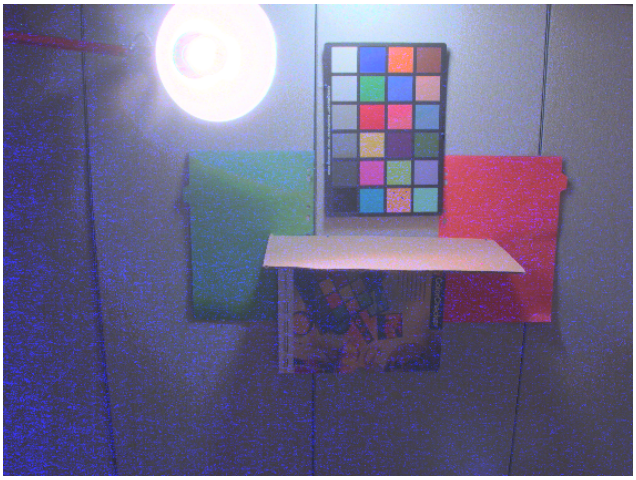

Fig. 20. HDR image composed and tone mapped from the noisy (ISO 800) sequence in RGB color space.

Fig. 21. HDR image composed and tone mapped from the noisy (ISO 800) sequence in luminance-chrominance (opponent) color space.